VERIZONA PUBLISHER
Publishing Your Ideas

www.verizonaonlinepublishing.com
Special Issue

Material Science and Engineering with Advanced Research

Solid Particle Erosion of Aluminum In-Situ Reinforced with a Cobalt Aluminide

K Lentzaris, AG Lekatou*, A Ntoumazios, AE Karantzalis and AK Sfikas

Laboratory of Applied Metallurgy, Department of Materials Science & Engineering, University of Ioannina, 45110 Ioannina, Hellas

***Corresponding author:** AG Lekatou, Laboratory of Applied Metallurgy, Department of Materials Science & Engineering, University of Ioannina, 45110 Ioannina, Hellas, Greece; Tel: (+30) 2651007309; Fax: (+30) 2651007309; E mail: alekatou@cc.uoi.gr

Article Type: Research, **Submission Date**: 19 February 2017, **Accepted Date:** 07 March 2017, **Published Date:** 18 May 2017.

Citation: K Lentzaris, AG Lekatou, A Ntoumazios, AE Karantzalis and AK Sfikas (2017) Solid Particle Erosion of Aluminum In-Situ Reinforced with a Cobalt Aluminide. Mater. Sci. Eng. Adv. Res Special Issue: 19-25. doi: https://doi.org/10.24218/msear.2017.3S.

Abstract

The present effort studies the comparative solid particle erosion behaviour of Al-Co alloys of various compositions in the Al-Al_9Co_2 side of the Al-Co phase diagram. The alloys have been prepared by vacuum arc melting. The main concept behind the selection of the Al-Al_9Co_2 region of the Al-Co phase diagram was the attainment of a two-phase structure (Al + Al_9Co_2) that could combine the beneficial attributes of Al_9Co_2, as a Complex Metallic Alloy in-situ reinforcement, with the ductility/toughness of Al, as a matrix to the brittle intermetallic.

Hypereutectic Al-Co alloys of various Co contents (7, 10, 15 and 20 wt.% Co), as well as monolithic commercially pure Al, were prepared by vacuum arc melting. The alloys were subjected to solid particle erosion testing at two impact angles (60° and 90°). The test results were interpreted based on weight change measurements and scanning electronic microscopy. It was revealed that the governing mechanisms change as the impact angle and the reinforcement volume fraction change. It was shown that factors affecting the brittle/ductile character of the material, such as Al_9Co_2 volume fraction, Al_9Co_2 coarseness, Co dissolved in Al, play a primary role on the erosion response of the alloys. The Al-Co alloys showed higher wear rates than Al. The wear rate increased with Co and, consequently, Al_9Co_2 increasing. The surface characteristics and degradation mechanisms are being discussed.

Keywords: Al–Co alloys, In-situ composites, Al-Al_9Co_2, Solid particle erosion.

Introduction

High-performance materials of today are required to possess a combination of properties such as thermal and wear resistance, chemical stability and inertness, corrosion resistance as well as excellent mechanical properties. The intermetallic compounds have long been recognized as potentially useful structural materials for high temperature applications [1]. Despite the significant research interest in the intermetallic compounds of Al, only few studies have been devoted to cobalt aluminides, possibly due to their limited, until recently, application potential. Co-aluminides may find applications as active heterogeneous catalysts [2], metallization layers in III-V semiconductor devices [3], to hydrogen fuel cell technologies [4] etc. Recently, the development of a new category of materials, that of Complex Metallic Alloys (CMAs)–Quasi Crystals (QCs) [5] has rekindled the interest in the Al-Co system: CMAs constitute a new class of intermetallic compounds with high structural complexity, giant unit cells containing from tens to more than a thousand atoms and lattice parameters of several nanometers [6]. CMAs have a rising potential as multifunctional materials due to properties, such as low surface energy associated properties (oxidation, corrosion and friction resistance, hydrogen sorption capacity), high hardness, low electrical conductivity and low thermal conductivity [7-11]. However, their low ductility limits their application potentials. The development of two- or multi-phase structures based on a soft metallic phase is considered a promising solution for overcoming the low temperature ductility of CMAs [12]. According to the Al-Co phase diagram [13], Al forms with Co several intermetallic (IC) phases, among which, various allotropic forms of $Al_{13}Co_4$have CMA structures(approximants to decagonal QCs). The monoclinic Al_9Co_2 is also a CMA with an intermediate structural complexity between B2-AlCo and the decagonal Al-Ni-Co quasicrystal [14].

Previous works by the authors [15-17] have found a notable improvement in the corrosion and wear resistance of Al in-situ reinforced with Al_9Co_2 and $Al_{13}Co_4$ CMA phases. Even low amounts of Co (2-7 wt.%) can significantly benefit the corrosion and sliding wear resistance of Al. Among Al-Co alloys prepared by vacuum arc melting (VAM), casting and free sintering, the former have exhibited superior microstructure in terms of uniformity and fineness that has led to superior corrosion and sliding wear performance [15]. On the above grounds and considering that the erosion response of Al-alloys, MMCs (Metal Matrix Composites), ICs and CMAs has become an important aspect of their application potential [18-23], the present work examines the solid particle erosion response of Al-Co in-situ composites prepared by VAM and compares it with that of commercially pure Al (CP-Al) also prepared by VAM(Al-VAM).

Materials and Methods

CP-Al and Al-Co alloys (7, 10, 15, 20 wt.% Co) were prepared by vacuum arc melting (VAM). Appropriate mixtures of Al powder (-44 μm, 99.5% purity) and Co powder (-37 μm, 99.5% purity), of 3.8-4.0 g weight, were placed in the cavity of the water-cooled copper base of a VAM furnace. The furnace chamber was closed, evacuated and, then, filled up with Ar. Arc was initiated and maintained using a W electrode with a direct current of 120 A. The solidified drops had the shape of a meniscus.

Specimens were cut from each produced meniscus, mounted and prepared for metallographic examination by standard metallographic procedures. Inspection of all samples was performed by Scanning Electron Microscopy (SEM) with the use of a Jeol JSM 6510 LV SEM equipped with an Oxford Instruments X-Act EDX (secondary electron (SE) and back scattered electron (BSE) modes).

Solid Particle Erosion (SPE) experiments were carried out at impact angles of 60° and 90° using angular Al_2O_3 particles (170 - 250 μm) as the erodent medium. Coupons were cut with a diamond saw, ground to 1200 grit and then were placed on the adjustable sample holder at the opposite side of the nozzle. The distance between the nozzle and the specimen was 10±1 mm. The pressure of the sprayed erodent from the nozzle, directly on the surface of the sample, was 3.5 bar. The duration of each spraying was 2 min. Every 10 s, the material loss was recorded. The overall erosion rate was calculated from the mass loss versus the erodent mass of the experiment (triplicate runs) by linear regression analysis (least squares method). Erosion was quantified by mass loss measurement with an accuracy of 0.1 mg.

Results and discussion

Microstructure of the alloys

Figure 1 illustrates the microstructures of the alloys, as fabricated. Extensive microstructural analysis of the examined alloys is presented elsewhere [16]. All alloys are composed of Al_9Co_2 phase uniformly distributed within an Al matrix. As the Co content of the alloy increases, the fraction of Al_9Co_2 increases. More analytically, the compositions of Al-7wt.%Co, Al-10wt.%Co, Al-15wt.%Co, Al-20wt.%Co, correspond to the Al_9Co_2 volume fractions of 36, 41, 50 and 63 vol.%, respectively [16].

The microstructure of the Al-7wt.%Co and Al-10wt.%Co appears almost entirely eutectic with directionality. A likely explanation for the excessive extent of the eutectic morphology, even though the employed compositions are hypereutectic, is that rapid cooling has largely suppressed the pre-eutectic stage, not allowing the primary Al_9Co_2 crystallites to grow. Especially in the case of Al-7 wt.% Co, fine plates of Al_9Co_2 are distributed in the ductile matrix in a uniform and highly ordered/orientated pattern.

In the case of Al-15 wt.%Co, a planar Al_9Co_2 phase is observed

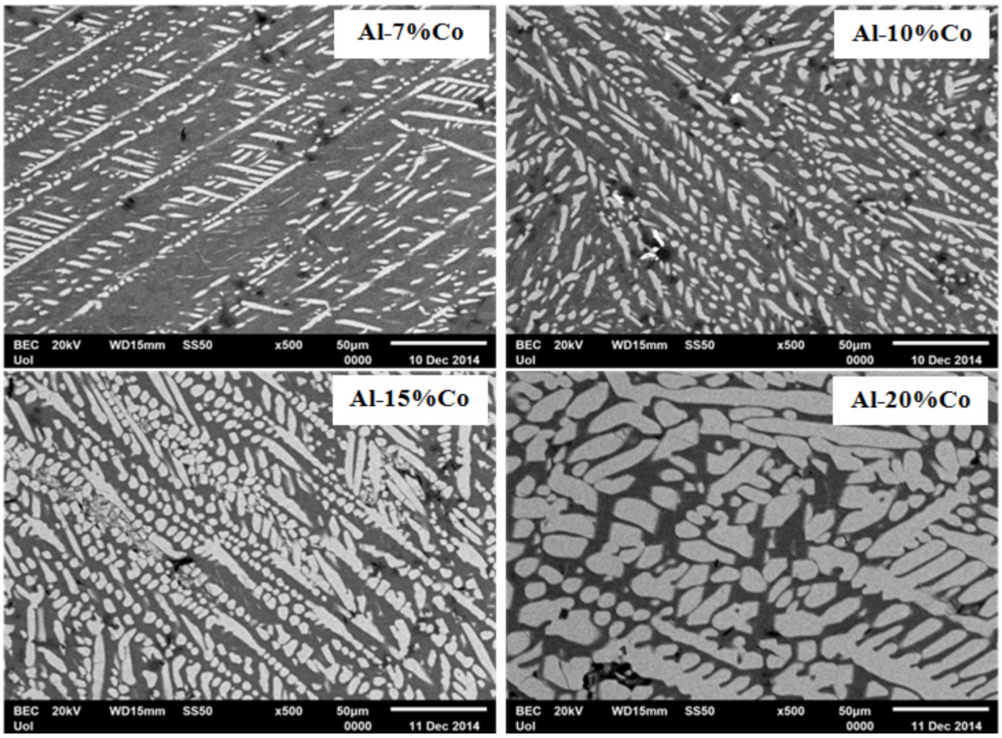

Figure 1: Microstructure of the Al-Co alloys, as fabricated (BSE mode)

to coexist with the Al-Al_9Co_2eutectic microconstituent. It can be observed that the Al_9Co_2 eutectic stripes are not continuous. Instead, they consist of small building brick-like units that form a directional pattern. It seems like the Al_9Co_2 phase was to grow in a continuous mode of directional stripes that were eventually chopped off in small units. The reason for such development mode can be sought in the continuous decrease in the necessary under cooling for the Al_9Co_2 eutectic stripe development as eutectic reaction {Al(l)→Al(s)+Al_9Co_2(s), 657°C} progresses [24-25]. This discontinuous pattern of Al_9Co_2 phase has also been observed in different types of composite materials fabricated by VAM [26-28].

In the case of Al-20 wt.% Co, a different morphology is observed: The intermetallic phase is in the form of coarse particles and blades. This morphology indicates the possibility of extensive pre-eutectic Al_9Co_2 presence, in consistency with Sater et al [29]. It seems that, in the case of high Co concentration, the pre-eutectic stage cannot be suppressed (due to the low conductivity of Al_9Co_2 CMA) and the growth of coarse primary Al_9Co_2 is favored. An alternative explanation for the presence of coarse primary Al_9Co_2 in the microstructure of RS Al-Co considers the instability of the supersaturated (in Co) solid solution: As Co content increases, the RS-due trapped Co in the αAl lattice increases (Previous work showed that the maximum dissolved Co in the Al matrix of Al-7 wt.% Co (0.59 wt.%) rose to 5.1 wt.% in Al-20 wt.% Co [16]). Due to the high contents of Co, the supersaturated α-solid solution is so unstable that, during cooling, the solute is rejected and builds up to the level required for the formation of the intermetallic phase [30].

To conclude, as the Co content increases, the amount of coarse primary Al_9Co_2increasesat the expense of fine-sized eutectic Al_9Co_2.

Solid particle erosion behaviour

Solid particle erosion rate: Figure 2, demonstrates the mass losses of the different composites as a function of the mass of the erosive medium at the impact angles of 60° and 90°. Figures 2a and 2b show that, as the erosive mass increased, the mass loss also increased, in compatibility with previous investigations [31-35]. It is well known that there is a dramatic difference in the response of ductile and brittle materials when the mass loss in erosion is measured as a function of the angle of impact. As stated by other researchers [36-40], ductile materials exhibit a maximum in the erosion rate at intermediate impact angles (15°,

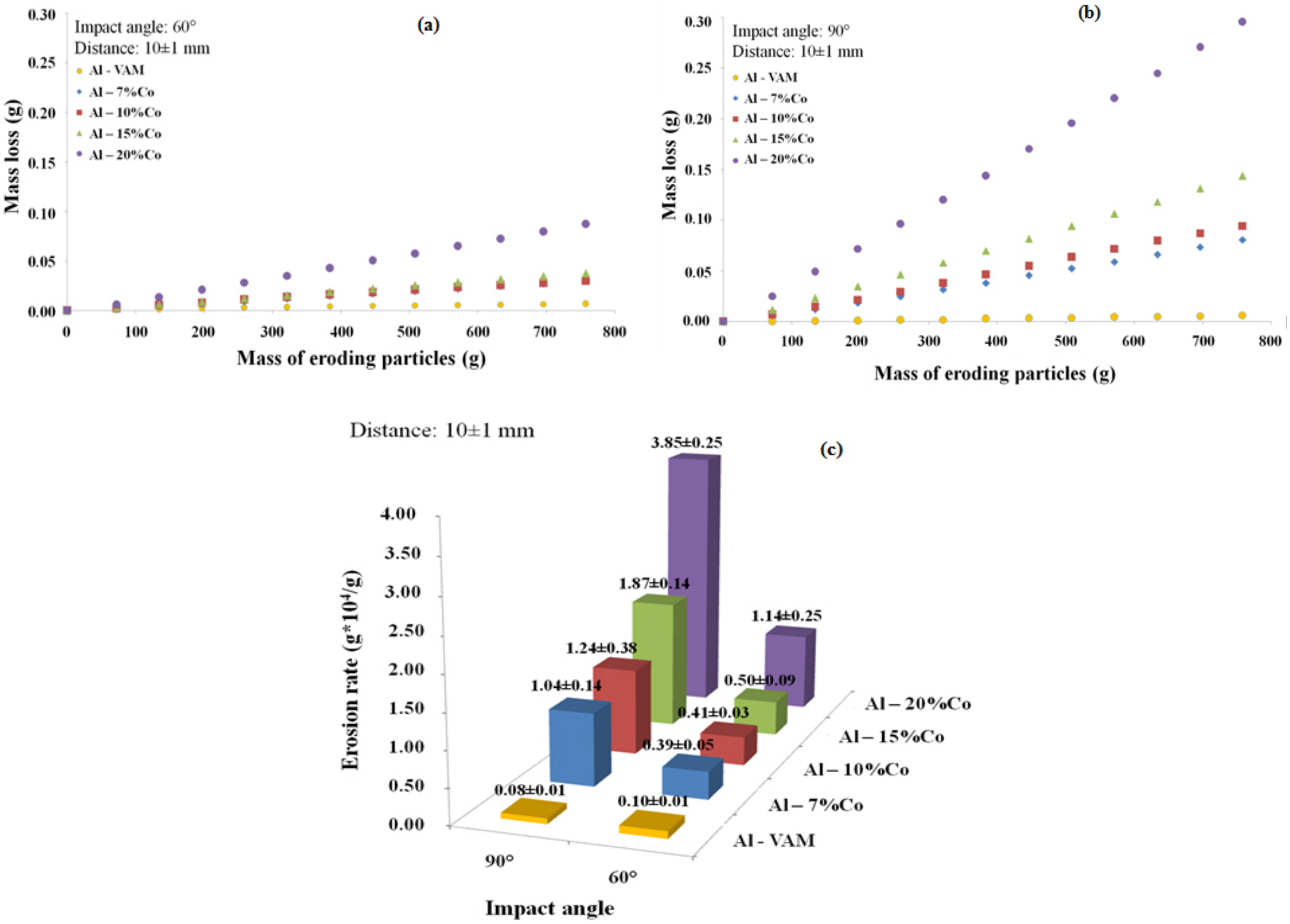

Figure 2: (a), (b) Mass loss versus mass of eroding particles during solid particle erosion testing at (a) 60° and (b) 90° impact angles; **(c)** the extracted erosion rates for Al-VAMand Al-Co alloys

30°). In contrast, the maximum erosion rate of a brittle material is usually obtained at higher impact angle (90°).

The erosion rate of the produced materials is displayed in Figure 2c. It can be observed that the erosion rate of Al-VAM is higher at the impact angle of 60° (as compared to that at 90°), whereas the produced alloys exhibit higher erosion rates at 90° (as compared to those at 60°). This behaviour can be explained by the fact that the monolithic ductile alloy principally erodes by abrading the surface. At low impact angles, the particles strike the surface, form a crater and then leave the surface. Material removal takes place more easily at a relatively low impact angle (60°) owing to ploughing and cutting by theAl_2O_3 particle flow. At a higher impingement angle (90°), however, the impact of theAl_2O_3 particle flow on the specimen surface may result in work hardening of the surface, higher subsurface deformation, less efficient ploughing and cutting, and thus, less material removal, as also observed by previous researchers [32,41]. Erosion mainly occurs by propagation and intersection of cracks caused by impacting particles. In other words, Al-VAM as a ductile material, has a low resistance to the shear stresses (responsible for ploughing), induced by the horizontal component of the impact force. On the other hand, Al-VAM as a ductile material, has a high resistance to the vertical component of the impact force. For this reason, impact at 90^o, has led to a lower erosion rate than impact at 60^o.

On the other hand, the Al-Co alloys seem to exhibit a more brittle behaviour towards solid particle erosion, since their erosion rates are higher at 90° than at 60°. The brittle constituent of the Al-Co alloy (i.e. Al_9Co_2) is more susceptible to the action of the vertical component of the impact force, thus being mainly responsible for the lower erosion resistance of the Al-Co alloys at 90° impact angle as compared to the resistance at 60° impact angle. Moreover, the depth of damage accumulation is largest in the alloys subjected to erosion at 90°, where the impact energies are almost totally absorbed through straining of the subsurface material [32].

In general, Figure 2 shows that:

(a) As the Co content increases, the erosion rate notably increases, especially in the case of Al-20wt.%Co impacted at 60°. This increase is owing to: (i) the increase in the amount and coarseness (i.e. surface area) of Al_9Co_2 (compare the coarse blades observed in the microstructure of Al-20 wt.% Co with the fine, uniformly distributed particles in the microstructure of Al-7 wt.% Co, in Figure 1), and (ii) the increase in the Co dissolved in the Al-matrix by RS, as aforementioned in the Microstructure section. Factors (i) and (ii) lead to an increase in the alloy brittleness with Co content increasing and, consequently, a decrease in the alloy capacity to absorb the impact energy as the Co content increases.

(b) Lower Co additions (7, 10 and 15 wt.% Co) exhibit erosion rates of the same order of magnitude per impact angle. The much higher erosion rate of Al-20 wt.% Co, in relation to the erosion rates of the 7-15 wt. %Co compositions, is mostly explained by the notably increased coarseness of the Al_9Co_2 plates and blades, as manifested in Figure 1. Further explanations are given in the following section, in context with the morphology of the eroded surfaces.

(c)Al-VAM exhibits much lower wear rate than that of the Al-Co alloys, attributed to its intensive plastic deformation. The unreinforced alloy presents the highest fracture energy and, therefore, the least mass loss. This is especially shown at the impact angle of 90°, where material removal by ploughing is minimal, as aforementioned.

In conclusion, for Al-VAM, the role of the cutting component of sharp-edged particles moving along the surface is shown to be substantial, whereas for the Al-Co alloys, the component of the impact force, which is perpendicular to the surface, has a predominant effect.

Eroded surface morphology: Figures 3 and Figure 4 reveal the morphology of the eroded surfaces for the different materials impacted at different angles (60° and 90°, respectively). An intensive landscape with extended and deep grooves, dimples and craters can be observed in the cases of 0-10 wt.% Co, which is characteristic of severe plastic deformation. It is evident that Al-VAM presents the highest frequency of plastic deformation signs, whilst Al-20 wt.%Co the lowest. As the Co content increases, the landscape gives an increasing evidence of constrained plastic flow of the deformed metal matrix (resulting in loss of ductile behaviour). It should be noted that the morphological differences are slight in the cases of Al-7 wt.% Co, Al-10 wt.% Co and Al-15 wt.% Co; nevertheless, the aforementioned trends are still observed.

In order to explain the erosion behaviour of the examined materials, certain issues should be taken into consideration. Impact of the eroding particles at 60° is a process that involves both the contribution of the outer surface and the substrate bulk material of the specimens. The surface of soft monolithic Al-VAM suffers severe plastic deformation from the particle impact leading to the formation of intensive grooves with subsequent side-flaw of material. The particles strike the surface, form a crater and then leave the surface. Some of the particles remove a chip as in metal cutting, while others leave material piled up at the sides of the crater. This uplifted material is presumably removed relatively easily by the impact of subsequent particles, as stated by other researchers [32,39]. As the impact at 60° proceeds, these piled up areas will eventually be detached and removed from the substrate, making this detachment the dominant mass loss mechanism. On the other hand, the ductility of CP-Al ensures that a significant amount of the particle impact energy is absorbed by the substrate so that the material loss is somewhat restricted without being allowed to reach extreme values. That way, the relatively low erosion rates at 60° (as compared to the ones at 90°) are also explained.

Instead, impact of the eroding particles at 90° for Al-VAM, is a process that is characterized mainly by heavy plastic deformation caused by the vertical component of the impact force. Several

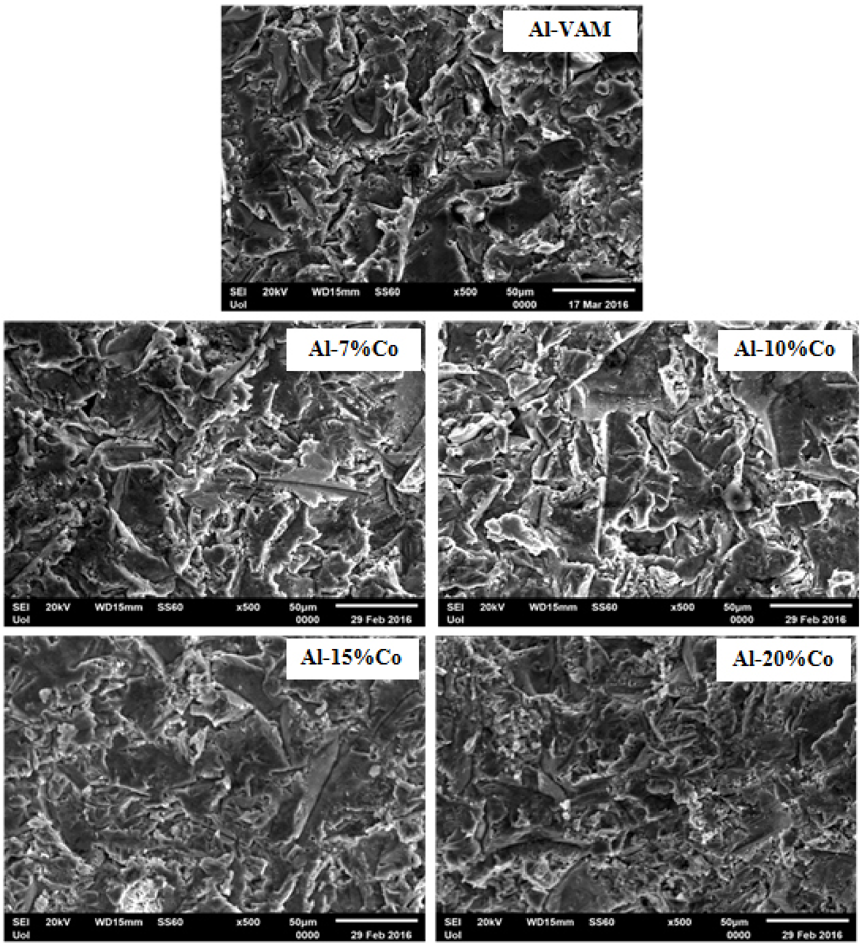

Figure 3: Morphology of the solid particle eroded surfaces at theimpact angle of60°(SE mode)

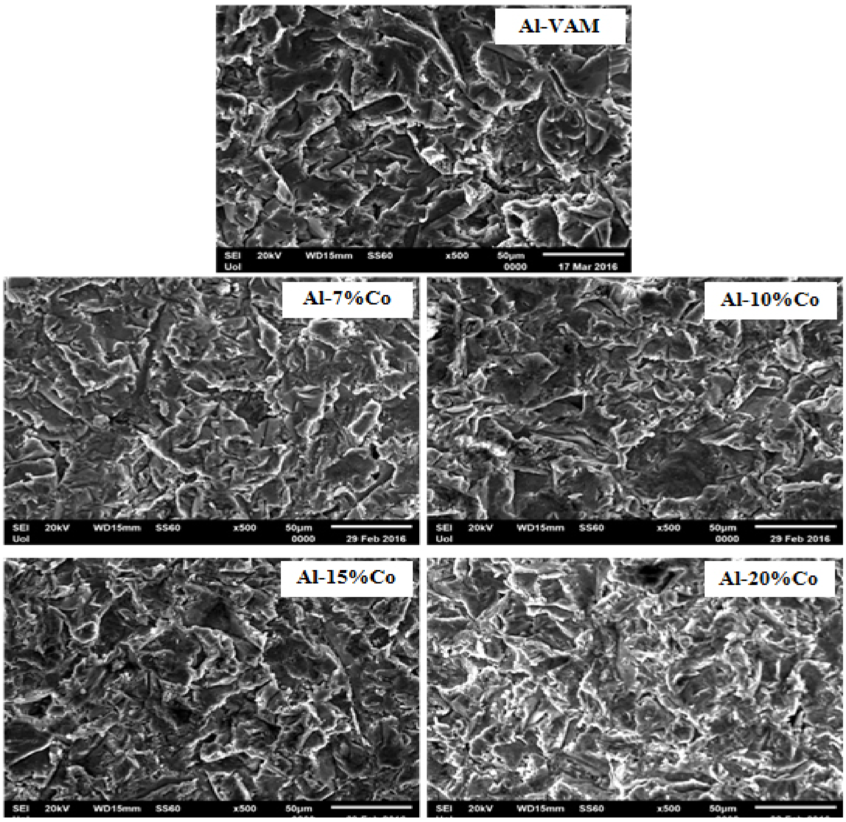

Figure 4: Morphology of the solid particle eroded surfaces at theimpact angle of 90°(SE mode)

other mechanisms have also been proposed for material removal at high impact angles. These include brittle behaviour due to work hardening, fragmentation of particles, low cycle fatigue, temperature effects due to high strain rates, delamination wear and extrusion mechanisms [42]. However, plastic deformation is still the governing mechanism. (A transition to micromachining or ploughing of material is observed at lower impact angles [43].)

The previous situation is notably altered with increasing the Co content and, consequently, the in-situ Al_9Co_2 reinforcement. As the Co content and, thus, the hard CMA amount increases, surface layers are hardened and plastic deformation is restrained. Hence, the ductility is reduced and a transition towards a more brittle behaviour is established.

It should be emphasized that an increase in the Co content results in a significant embrittlement of the alloy, not only due to the aforementioned increase in the amount of the Al_9Co_2 phase but also due to the coarsening of the Al_9Co_2 phase. Indeed, the coarsening of the microstructure of the Al-Co alloys seems dramatic in Al-20 wt.%Co, as manifested in Figure 1. In addition, the Al matrix becomes less ductile with Co content increasing, because RS has led to an increasing Co dissolution in Al with Co content, as already mentioned in the Microstructure section; the dissolved Co in Al is much greater than the insignificant solubility of Co in Al under equilibrium [13]. Furthermore, pores within coarse Al_9Co_2 plates and sharp edges of blades are stress concentration points promoting crack formation. As Co increases, stress concentration points—such as Al_9Co_2 blade and acicular plate tips, angles between Al_9Co_2 dendrite arms, intersections of dendrites and dendrite arms increase [16], features mostly discerned in the micrograph of Al-20 wt.% Co (Figure 1). As such, at higher Co contents, the residual stresses of the RS alloys are higher as compared to lower Co contents. Therefore, as displayed in Figures 3 and 4, erosion at high Co contents mainly occurs by the propagation and intersection of cracks induced by impacting particles. As embrittled materials, the Al-Co alloys of high Co content have reduced capacity to absorb the impact energy; consequently, the impact energy generates high impact loads on the surface, which accordingly lead to significant material loss, especially in the case of the most brittle alloy (Al-20wt.%Co) eroded at 90°.

Conclusions

CP-Aland Al-Co alloys (7, 10, 15, 20 wt.% Co) were prepared by vacuum arc melting. The alloys were composed of Al_9Co_2 particles uniformly distributed in an Al matrix. By increasing the Co content of the alloy, the fraction and coarseness of Al_9Co_2 increased; the shape of the Al_9Co_2 phase changed from fine plate arrays to coarse plates and blades.

The solid particle erosion behaviour of CP-Al (Al-VAM) and Al-Co alloys has been demonstrated. All Al-Co compositions showed lower resistance to solid particle erosion at 60° and 90° impact angles than Al-VAM, attributed to the increasing embrittlement of the materials with Co increasing (and, hence, Al_9Co_2 content, Al_9Co_2 coarseness and Co dissolved in Al increasing).

The erosion rate of CP-Al at the impact angle of 90° was lower than that at 60°, since the horizontal component of the impact force is mostly responsible for the ductile material removal by ploughing and cutting.

The erosion rate of the Al-Co alloys at the impact angle of 60° was lower than that at 90°, since the vertical component of the impact force (that mostly affects brittle materials, such as Al_9Co_2) was reduced.

The main degradation mechanisms identified are: For Al-VAM: Intensive plastic deformation in the form of grooves, dimples, craters and ploughing; For Al-Co alloys: Plastic flow constraint, crack propagation and intersection causing fracture and removal mostly of Al_9Co_2 phase.

Further work is under way to obtain a better fundamental understanding of erosion wear at lower impact angles (30° and 45°) with an attempt to find a general law for rapidly solidified systems such as Al-Co alloys, in order to improve their erosion resistance.

Acknowledgments

The authors would like to acknowledge Prof. S. Makridis for applying part of the arc-melting apparatus system under his patent: https://www.researchgate.net/publication/200664162_Multiapparatus_Arc_Melting_for_Rapid_Solidification_Processes?ev=prf_pub, as well as Ms. A. Poulia for her help in obtaining the SEM photos.

References

1. Pope DP, Darolia R. High-temperature applications of intermetallic compounds. MRSBull. 1996; 21(5):30-36.
2. Yamauchi I, Kawamura H, Nakano K, Tanaka T. Formation of fine skeletal Co-Ag by chemical leaching of Al-Co-Ag ternary alloys. J. Alloy Compd. 2005; 387(1-2):187-192. doi: http://dx.doi.org/10.1016/j.jallcom.2004.06.048.
3. Tanaka M, Ikarashi N, Sakakibara H, Ishida K, Nishinaga T. Atomic-scale morphology and interfaces of epitaxially embedded metal (coal)/semiconductor (GaAs/AlAs) heterostructures. Appl. Phys. Lett. 1992; 60(7):835-837.
4. Armbrüster M, Schlögl R, Grin Y. Intermetallic compounds in heterogeneous catalysis – a quicklydeveloping field. Sci Technol Adv Mater. 2014; 15(3):034803.
5. Dubois JM, Belin Ferré E, Feuerbacher M. Introduction to the Science of Complex Metallic Alloys, in Complex Metallic Alloys: Fundamentals and Applications. DuboisJM, Belin-Ferré E, editors. Wiley-VCH; 2011. p.1–39.
6. Urban K, Feuerbacher M. Structurally complex alloy phases. J. Non-Crystal. Solids. 2004; 334–335:143–150. doi: http://dx.doi.org/10.1016/j.jnoncrysol.2003.11.029.
7. Barthes Labrousse MG, Dubois JM. Quasicrystals and complex metallic alloys: Trends for potentialapplications. Philos.Mag. 2008; 88(13-15):2217-2225. doi: http://dx.doi.org/10.1080/14786430802023036.
8. Dubois JM, Belin-Ferré E. Friction and solid-solid adhesion on complex metallic alloys. Sci Technol Adv Mater. 2014; 15(3):034804.

9. Rabson DA. Toward theories of friction and adhesion on quasicrystals. Prog. Surf. Sci. 2012; 87(9-12):253–271. doi: http://dx.doi.org/10.1016/j.progsurf.2012.10.001.
10. Thiel PA. Quasicrystal Surfaces. Annu. Rev. Phys. Chem. 2008; 59:129-152.
11. Maciá E. The role of aperiodic order in science and technology. Rep. Prog. Phys. 2006; 69:397–441.
12. Eckert J, Scudino S, Stoica M, Kenzari S, Sales M. Mechanical engineering properties of CMAs in Complex Metallic Alloys: Fundamentals and applications. DuboisJM, Belin Ferré E, ediotrs. Wiley-VCH; 2011. p. 273–315.
13. McAlister AJ. The Al-Co (Aluminum-Cobalt) system. Bull. Alloy Phase Diagr. 1989; 10(6):646-650.
14. Alarcon Villaseca S, Ledieu J, Serkovic Loli LN, De Weerd MC, Gille P, Fournée V, et al. Structural investigation of the (001) surface of the Al_9Co_2 Complex Metallic Alloy. J. Phys. Chem. C. 2011; 115(30):14922–14932.
15. Lekatou A, Sfikas AK, Karantzalis AE, Sioulas D. Microstructure and corrosion performance of Al-32%Co alloys. Corros. Sci. 2012; 63:193-209.
16. Lekatou A, Sfikas AK, Petsa C, Karantzalis AE. Al-Co alloys prepared by vacuum arc melting: correlating microstructure evolution and aqueous corrosion behaviour with Co content. Metals. 2016; 6(3):46. doi: http://dx.doi.org/10.3390/met6030046.
17. Sfikas AK, Lekatou A, Karantzalis AE. Sliding wear behaviour of rapidly solidified Al-Co alloys. 17th Int. Conf. on Experimental Mechanics (ICEM 17); 2016 July 3-7; Rhodes, Greece.
18. Pasha M, Kaleemulla M. Erosive wear behaviour of sprayed metal matrix composites: An overview. J. Eng.Tribol. 2013; 227(10):1063-1075.
19. Takaffoli M, Papini M. Numerical simulation of solid particle impacts on Al6061-T6. Part II: Materials removal mechanisms for impact of multiple angular particles. Wear. 2012; 296(1-2):648-655. doi: http://dx.doi.org/10.1016/j.wear.2012.07.022.
20. Alman DE, Hawk JA, Tylczak JH, Dogan CP, Wilson RD. Wear of iron-aluminide intermetallic-based alloys and composites by hard particles. Wear. 2001; 251(1-12):875-884. doi: http://dx.doi.org/10.1016/S0043-1648(01)00745-1.
21. Miyazaki N. Solid particle erosion of composite materials: A critical review. J. Compos. Mater. 2016; 50(23):3175-3217.
22. Peat T, Galloway A, Toumpis A, McNutt P, Iqbal N. The erosion performance of particle reinforced metal matrix composite coatings produced by co-deposition cold gas dynamic spraying. Appl. Surf. Sci. 2017; 396:1623-1634.
23. Chowdhury MA, Debnath UK, Nuruzzaman DM, Islam Md M. Experimental analysis of aluminum alloy under solid particle erosion process. Proceedings of the Institution of Mechanical Engineers, Part J: J. Eng. Tribol. 2016; 230(12):1516-1541.
24. Jackson KA. Crystal-growth kinetics. Mater. Sci. Eng. 1984; 65(1):7-13. doi: http://dx.doi.org/10.1016/0025-5416(84)90194-0.
25. Jackson KA. The interface kinetics of crystal growth processes. Interface Sci. 2002; 10:159–169. doi: 10.1023/A:1015824230008.
26. Karantzalis AE, Lekatou A, Georgatis E, Arni Z, Dracopoulos V. Solidification observations of vacuum arc melting processed Fe-Al-TiC composites: TiC precipitation mechanisms. Mater. Character. 2011; 62(12):1196-1204. doi: http://dx.doi.org/10.1016/j.matchar.2011.10.009.
27. Karantzalis AE, Lekatou A, Tsirka K. Solidification observations and sliding wear behaviour of vacuum arc melting processed Ni–Al–TiC composites. Mater. Character. 2012; 69:97-107. doi: http://dx.doi.org/10.1016/j.matchar.2012.04.013.
28. Karantzalis AE, Arni Z, Tsirka K, Evangelou A, Lekatou A, Dracopoulos V. Fabrication of TiC reinforced composites by Vacuum Arc Melting: TiC mode of re-precipitation in different molten metals and alloys. J. Mater. Eng. Perform. 2016; 25(8):3161-3172.
29. Sater JM, Sanders TH, Garrett RK. Characterization of rapidly solidified materialsin rapidly solidified powder aluminum alloys. ASTM STP. 1986; 890:83–117. doi: 10.1520/STP33025S.
30. Menon J, Suryanarayana C. Metallography of a melt-quenched aluminum-cobalt alloy. Metallography. 1988; 21(2):179-197. doi: http://dx.doi.org/10.1016/0026-0800(88)90015-8.
31. Tu JP, Pan J, Matsumura M, Fukunaga H. The solid particle erosion behavior of Al18B4O33 whisker-reinforced AC4C Al alloy matrix composites. Wear. 1998; 223(1-2):22-30. doi: http://dx.doi.org/10.1016/S0043-1648(98)00295-6.
32. Fang Q, Sidky P, Hocking MG. Erosive wear behaviour of aluminium based composites. Mater. Des. 1997; 18(4-6):389-393. doi: http://dx.doi.org/10.1016/S0261-3069(97)00081-2.
33. Ramesh CS, Shreeshail ML, Gudi HR, Zulfiqar K. Air jet erosion wear behavior of Al6061-SiC-Carbon fibre hybrid composite. Mater. Sci. Forum. 2014; 773-774:547-554.
34. Gousia V, Tsioukis A, Lekatou A, Karantzalis AE. Al-$MoSi_2$composite materials: Analysis of microstructure, sliding wear, solid particle erosion and aqueous corrosion. J. Mater. Eng. Perform. 2016; 25(8):3107-3120. doi: 10.1007/s11665-016-1947-1.
35. Miyazaki N, Funakura S. Solid particle erosion behavior of metal matrix composites. J. Compos. Mater. 1996; 30(15):1670-1682.
36. Hung FY, Chen LH, Lui TS. Impact angle of maximum erosion rate of wear resistant spheroidal graphite cast iron eroded by SiO_2 and Al_2O_3 particles. Int. J. Cast Metals Res. 2003; 16(5):505-513.
37. Lopez D, Congote JP, Cano JR, Toro A, Tschiptschin AP. Effect of particle velocity and impact angle on the corrosion-erosion of AISI 304 and AISI 420 stainless steels. Wear. 2005; 259(1-6):118-124. doi: http://dx.doi.org/10.1016/j.wear.2005.02.032.
38. Oka YI, Mihara S, Yoshida T. Impact-angle dependence and estimation of erosion damage to ceramic materials caused by solid particle impact. Wear. 2009; 267(1-4):129-135. doi: http://dx.doi.org/10.1016/j.wear.2008.12.091.
39. Finnie I. Some reflections on the past and future of erosion. Wear. 1995; 186-187(1):1-10. doi: http://dx.doi.org/10.1016/0043-1648(95)07188-1.
40. Sundararajan G, Roy M. Solid particle erosion behaviour of metallic materials at room and elevated temperatures. Tribol. Int. 1997; 30(5):339-359. doi: http://dx.doi.org/10.1016/S0301-679X(96)00064-3.
41. Wilson S, Ball A. Performance of metal matrix composites under various tribological conditions. In: Advances in Composite Tribology. Friedrich K, editor. Elsevier; 1993. p. 311-366.
42. Hutchings I, Winter RE. Particle erosion of ductile metals: A mechanism of material removal. Wear. 1974; 27(1):121-128. doi: http://dx.doi.org/10.1016/0043-1648(74)90091-X.
43. Wilson S, Ball A. Wear resistance of an aluminium matrix composite. In: Tribology of Composite Materials. Rohatgi PK, Blau PJ, Yust CS, editors. Metals Park, OH: ASM Int; 1990. p.103–112.